Relative sea level change in west Greenland during the last millennium

Antony J. Long[1], Sarah A. Woodroffe[1], Glenn A. Milne[2], Charlotte L. Bryant[3] and Leanne, M. Wake[4]

[1]Department of Geography, Durham University, Science Site, South Road, Durham DH1 3LE, UK
[2]Department of Earth Sciences, Ottawa University, Marrion Hall, Ottawa, K1N6N, Canada
[3]NERC Radiocarbon Laboratory, Scottish Enterprise Technology Park, Rankine Avenue, East Kilbride, Glasgow, G75 0QF, UK
[4]Department of Earth Sciences, Durham University, Science Site, South Road, Durham, DH1 3LE, UK

ABSTRACT

Relative sea level (RSL) data provide important long-term (century to millennial-scale) constraints on ice load history in Greenland. In this paper we present the results of a litho-, bio- and chronostratigraphic study designed to reconstruct RSL during the last millennium from salt marsh deposits recovered from a field site near to the town of Sisimiut. The stratigraphy at three marshes typically records an upwards transition from freshwater to salt marsh deposits. We use a quantitative (transfer function) and subjective model to reconstruct palaeomarsh elevation and changes in mean tide level (MTL) from 16 sediment profiles from these marshes. These palaeomarsh elevations are placed in a chronological framework established by 18 radiocarbon dated index points. Both models yield similar results and show MTL rose from -0.60 ± 0.20 m at c. 600 cal a BP to reach -0.10 ± 0.20 m at c. 400 cal a BP. After this time, MTL remained close to present (± 0.20 m) until the present day although low sedimentation rates limit the resolution of our reconstructions during this interval. The initial rise in RSL can be explained by the dominance of non-Greenland processes, notably the collapse of the Laurentide forebulge, over local (Greenland) solid Earth uplift caused by postglacial ice unloading. This is despite some reloading of the crust that occurred during the neoglacial expansion of the Greenland Ice Sheet in this part of west Greenland. The slow-down in RSL at 400 cal a BP does not record either a change in the rate of Laurentide forebulge collapse or a change in eustatic sea level. We argue instead that this slow-down records the effects of a sustained reduction in local (Greenland) ice mass that persists over most of the past 400 years. The latter interval is widely acknowledged as a period of generally cooler than present conditions associated with the later stages of the Little Ice Age. During this period, field evidence suggests that in many areas the ice sheet had reached its maximum late Holocene extent. It is not obvious at this stage how to reconcile an expanding ice sheet with a reduction in ice load during this interval although we hypothesise it could reflect one or more of; i) a change in ice sheet dynamics; ii) reduced mass accumulation caused by cold and dry conditions, and; iii) a lagged response to earlier periods of climate warming.

Keywords: Greenland Ice Sheet; relative sea level change; salt marsh; diatom; ice sheet models, glacio-isostatic rebound; transfer function

*Corresponding author
Antony J. Long (A.J.Long@Durham.ac.uk)
Tel: +44 191 334 1913
Fax: +44 191 334 1801

1. Introduction and aims

The Greenland Ice Sheet, like many other ice masses, expanded during the relatively cool 'neoglacial' that followed the early and mid Holocene thermal optimum, and reached a maximum recent extent during the Little Ice Age (Kelly, 1980; Porter, 2000; Wanner et al., 2008). Previous work in Greenland suggests that changes in neoglacial ice load had a direct impact on vertical land motions and associated relative sea level (RSL) change (Weidick, 1993). However, to date there exist only a handful of well-constrained geological estimates of RSL from Greenland during the last millennia and so models of neoglacial ice sheet history are poorly constrained.

Salt marshes provide a valuable source of late Holocene RSL data on temperate latitude coasts (Gehrels et al., 2006). Although salt marshes are common in west Greenland (Lepping and Daniëls, 2007) until recently their use for RSL study has not been attempted (Long and Roberts, 2002). Woodroffe and Long (2009a) present the results of an investigation into the contemporary salt marsh environments at Sisimiut (Figure 1) and develop a diatom-based transfer function that they then apply to a salt marsh sediment profile. Their work shows that the transfer function method can be applied to Greenland salt marshes to reconstruct recent RSL change and therefore potentially help constrain the history of the ice sheet during the last millennium.

In this paper we present the results of a litho-, bio- and chronostratigraphic investigation of RSL change during the last millennium from the same salt marshes near Sisimiut studied by Woodroffe and Long (2009). We use 18 radiocarbon dates from 16 sediment profiles to reconstruct a c. 0.60 m RSL rise between c. 600 and 400 cal a BP, after which RSL remained within a few decimeters of present. We argue that this slow-down is due to a reduction in local (Greenland) ice mass and the associated changes in land height and gravity through the glacial isostatic adjustment process. This conclusion is surprising since it implies that west Greenland lost mass during the Little Ice Age. Our work shows that this part of the Greenland Ice Sheet has undergone important changes in mass balance during the recent past and responds to climate change in a complex manner that we do not yet fully understand.

2. Models of relative sea level change in west Greenland during the last millennium

Therkel Mathiassen (in Gabel-Jørgensen and Egedal, 1940) is one of a number of archaeologists who describe evidence from west Greenland of Eskimo houses that have either been partly washed away by the sea or lie below the high water mark (Mikkelsen et al., 2008). The sea level significance of many of these archaeological records were synthesised by Weidick (1993) into a 'Th. M' and a 'Norse' model which show RSL rise of between 2 m and 6 m since c. AD 1200 (Figure 2). Weidick (1993) attributed this large rise in RSL in the last millennium to a progressive

build-up of ice during the Little Ice Age from AD 1300 onwards, as depicted by a glaciation curve for Disko Bugt.

More recent geological research confirms that RSL has risen in the late Holocene in west Greenland. In Disko Bugt (Figure 1), drowned isolation basins show that RSL in the eastern part of the bay rose by 1 m to 2 m during the last 2 k cal a BP (Long et al., 2003). Beach ridges and coastal lagoon sediment sequences on Disko Island record at least three transgressions in the last millennium, with sea level reaching close to present about 400 to 500 years ago (Rasch and Jensen, 1997; Rasch, 2000). In the Nanortalik area of south Greenland, Sparrenbom et al. (2006) and Mikkelsen et al. (2008) suggest that RSL also rose throughout the late Holocene at a rate of 1 m to 2 m per thousand years. Recent GPS observations confirm that areas close to the ice sheet margin throughout central west Greenland are subsiding by up to 4 mm yr, with rates of subsidence declining with distance from the ice sheet margin (Dietrich et al., 2005).

3. Study area

The study area is located 30 km south of the coastal town of Sisimiut (Figure 1b). The landscape is a low coastal plain dissected by many narrow tidal inlets. The tidal range is c. 4.5 m and mean high water of spring tides (MHWST) and highest astronomical tides (HAT) occur at +1.62 m and +2.33 m above mean tide level (MTL) (Royal Danish Administration of Navigation and Hydrography, pers. comm.). The annual mean temperature at Sisimiut (1949-1999) was -3.9 ± 2.8 °C and the study area is underlain by permafrost (van Tatenhove and Olesen, 1994). First year sea ice forms in the sheltered waters of the study area during the winter.

Woodroffe and Long (2009a) detail contemporary diatom distributions, macrophyte vegetation zones, particle size and organic content measured by % loss on ignition (%LOI) across three small salt marshes in the study area (Figure 1d). The contemporary diatom data are briefly reviewed in the following section because they inform our interpretation of the fossil sequences that are the focus of this paper. Locally the transition from upland vegetation comprising *Empetrum nigrum* heath or freshwater marsh to high marsh vegetation comprising *Cares glareosa* occurs at 2.50 ± 0.13 m MTL (Figure 3). The high marsh extends downwards to 1.74 ± 0.30 m, close to the level of MHWST where it grades into low marsh dominated by *Puccinellia phyryganodes*. The low marsh has a minimum measured elevation of 0.27 m MTL where tidal flat begins. Organic content expressed by percentage loss on ignition (%LOI) is generally high (>40%) above 1.90 m and falls below this elevation. The surface sediment of the marshes comprises sand-rich silts with some clay. Below the level of MHWST the marsh sediments are typically 60-80% sand, 20-40% silt and 0-10% clay, regardless of elevation. Above MHWST the pattern is more varied and probably records input of material from upland sources to the upper marsh (Woodroffe and Long, 2009a).

4. Methods of reconstruction

We excavated shallow trenches through the salt marshes by spade to expose sediment sequences. All samples were surveyed to MTL by levelling to a temporary benchmark which we related to local tidal levels measured by a sea bed pressure transducer during our fieldwork. We compared these data to tidal predictions for the same period at Sisimiut (Royal Danish Administration of Navigation and Hydrography, pers. comm.). During a 10-day period there was a 0.02 m average difference in the high and low tides between observed levels at our field site and predicted levels at Sisimiut. There was a 0.01 m error in our levelling between the temporary benchmark, the sample sites and local tide level, and a 0.03 m difference between our measured tide levels and those recorded by the local pressure transducer (based on three measurements made during a tidal cycle). Based on these observations we adopt a conservative error of ± 0.05 m for our tidal data. Where possible we sampled thin (c. 10 cm) sediment sequences that overlie bedrock to minimise any potential effects of frost heave and sediment compaction. We cut sample blocks from cleaned sections with a knife, wrapped them in plastic and returned them to Durham University for laboratory analysis.

We prepared samples for fossil diatom analysis from our sample sequences using standard techniques (Palmer and Abbott, 1986) with 250 diatom valves counted in most samples. Samples for particle size analysis (PSA) were analysed using a Coulter lazer particle size granulometer, after pretreatment with hydrogen peroxide to dissolve organic material. %LOI was calculated by weighing and burning 5 g of dry sediment in a furnace at 550°C for four hours (Heiri et al., 2001).

We reconstruct palaeomarsh elevation with a transfer function, a mathematical model that uses contemporary diatom distributions to predict the palaeomarsh surface elevation at which a fossil diatom assemblage formed. A training set of contemporary diatom data from the local salt marshes studied is described by Woodroffe and Long (2009a). The main diatoms at the top of the high marsh are *Pinnularia intermedia* and *Pinnularia borealis* (Figure 4) and are replaced close to HAT by *Navicula pusilla, Nitzschia palea* and *Eunotia praerupta*. Between HAT and MHWST frequencies of *Pinnularia microstauron, Caloneis borealis, Nitzschia sigma* and *Navicula salinarum* dominate. The tidal flat, close to MTL, supports a mixture of poly- and mesohalobian species including *Achnanthes delicatula, Opephora marina* and *Navicula forcipata*. The transfer function used in this paper is the 'pruned' model of Woodroffe and Long (2009a) in which four samples and eight taxa are removed as outliers from the contemporary training set (Figure 5). The resulting model has a good fit between observed and predicted elevation (r^2 = 0.94). Using weighted averaging partial least squares (WA-PLS) regression the training set produces a model with a root mean squared error of prediction (RMSEP) of 0.19 m at the second WA-PLS component.

An attraction of the transfer function (TF) method is its ability to predict palaeomarsh surface elevation for every diatom level counted from our salt marsh sequences. However, TFs treat each sample in isolation and cannot take advantage of environmental information contained in the samples immediately below or above the target level. Such information can provide useful constraints when reconstructing palaeomarsh surface elevations. Also, our TF only uses diatom data and as such is blind to any trends in stratigraphy, as measured by %LOI or with grain size data. Therefore, alongside the TF we use a visual assessment (VA) method that interprets key changes in diatom taxa and these additional stratigraphic data to reconstruct palaeomarsh surface elevation (Table 1).

The VA method places emphasis on changes in multiple taxa that occur across relatively narrow height ranges, taking into account the overall ecological succession indicated by the fossil and the contemporary diatom data (Table 3). For example, for a fossil sample containing >5% of *Pinnularia microstauron* and *Pinnularia intermedia,* the palaeomarsh surface elevation can be constrained by the modern distributions of these two taxa (Figure 4) which both have small vertical ranges in the upper part of local modern marshes. Their combined vertical ranges are limited to between 2.06 – 2.29 m MTL, giving a median palaeomarsh surface reconstruction of 2.17 ± 0.12 m MTL. With the VA approach we extend this approach to other major taxa with small tolerances, taking into account presence and absence of these taxa and vertical trends within these taxa (e.g., species abundances falling or rising) through each section.

The VA approach works best in the upper marsh where the major taxa occupy a small vertical zone. However, the height uncertainties in this method increase in low marsh settings where oligohalobian-halophile and mesohalobian taxa (e.g., *Navicula cincta*, *Navicula peregrina*, *Navicula salinarum* and *Nitzschia sigma*) with wider salinity tolerances dominate (Figure 4), although where possible we avoided dating these levels and instead focussed on samples from higher in the tidal frame. A potential strength of the VA method is the common sense, subjective interpretation of several lines of evidence to interpret each sequence. It is easy to be critical of such an approach, given the apparently greater rigour provided by the TF method. But the TF method is also based on several subjective decisions, including which taxa or samples to leave out of contemporary training sets, the length of the environmental gradient itself, as well as the particular statistical model used in the TF (e.g. WA-PLS).

A chronology for our sediments is developed with 21 AMS radiocarbon dates. We collected material for dating by sieving 1-cm thick sediment samples and extracting under microscope plant macrofossils, mainly *Empetrum nigrum* seeds and leaves and Cyperaceae seeds (Table 2). These were cleaned to remove adhering organic material and dried before being dated at the NERC

Radiocarbon Laboratory and SUERC AMS Laboratory in East Kilbride, Scotland. Dates are calibrated using the Oxcal calibration program (v. 4, Bronk Ramsey, 1995; 2001) and ages are cited in calibrated years Before Present (cal a BP). Radiocarbon dates are cited with a one sigma age error and, unless stated otherwise, all calibrated dates are quoted with a two sigma calibrated age range.

5. Results

5.1 Fossil sequences

We collected stratigraphic data from three salt marshes (A-C) (Figure 1d). Typically the stratigraphic sequences record freshwater peat overlain by salt marsh sediment. Each sequence generated at least one dated sea level index point and each has diatom counts at 1 cm intervals across the transition from freshwater peat and extending to the present marsh surface. We now describe two representative profiles from each marsh and provide full details of the remaining 11 diatom sequences as on-line supplementary information.

5.1.1 Marsh A2

Marsh A2 comprises a tidal flat and low marsh separated from an area of high marsh that grades into freshwater upland across a small bedrock ramp (Figure 6a). The sediments overlying the ramp and beneath the high marsh rest on bedrock, but the low marsh overlies unconsolidated silts and sands of uncertain depth. We trenched the low marsh to expose a wet, grey sandy silt that is overlain by a 10 cm-thick, red/brown peat with woody roots and abundant plant macrofossils (leaves, seeds and stems of *Empetrum*). This freshwater peat passes upwards into grey blue sands and silts with roots and occasional angular rock fragments that extend to the present marsh surface. We collected two monolith samples from the low marsh (Mono 7 and Mono 6, Figure 6a). The sediments on the ramp (Mono 4a, A2-3 and A2-4) comprise a thin, dark brown or black well-humified peat above bedrock which passes upwards into faintly laminated grey/brown organic silts and sands that extend to surface.

Mono 6 (Figure 6b)

Diatoms across the upper peat-sediment contact show the replacement of oligohalobous-indifferent taxa, notably *Pinnularia viridis* and *Pinnularia microstauron* by oligohalobous and mesohalobian taxa, dominated by *Navicula peregrina* and then *Navicula cincta*. %LOI falls from a maximum of 40% at 10 cm to <20% above 9 cm. Grain size data show that the salt marsh sediment is a sand with some silt. A sample of seeds and leaves of *Empetrum nigrum* and

Cyperaceae from 10-9 cm depth was dated to 640±48 ^{14}C yr BP (SUERC-13886, 662-559 cal a BP).

A2-4 (Figure 6c)

The stratigraphy comprises a dark brown humified peat that above 7 cm is overlain by a light brown sediment-rich peat with roots. Diatoms record the upwards replacement of oligohalobian-indifferent taxa in the peat (*Pinnularia intermedia*, *Pinnularia microstauron* and *Stauroneis anceps*) by oligohalobous (*Navicula cincta*) and mesohalobian taxa (*Navicula salinarum* and *Navicula peregrina*) in the overlying sediment. %LOI falls from 40-60% below 5 cm depth to <20% above this level. This fall corresponds with an increase in the sand content of the sediment. A sample of *Empetrum nigrum* seeds and leaves and Cyperaceae seeds from 8-7 cm depth was dated to 446±35 ^{14}C yr BP (SUERC-16540, 540-335 cal a BP).

5.1.2 Marsh A3

On the southern edge of Marsh A3 is a narrow sloping bedrock ledge that is overlain by salt marsh which has a surface elevation of between 1.95 and 1.55 m MTL (Figure 7). The stratigraphy of the marsh comprises a black humified peat that is overlain by a silt that contains sandy laminations and occasional angular rock fragments. We analysed four sediment profiles from the section; A3-4 is described in Woodroffe and Long (2009a) and below we detail profiles A3-6 and A3-3.

A3-6 (Figure 7b)

The sequence is a thin dark brown peat overlain at 4 cm by a grey brown silt sand with some laminations. The lowest diatom sample, taken directly above the bedrock, contains a polyhalobous assemblage with high frequencies of *Paralia sulcata* and *Plagiogramma staurophorum*. We believe these diatoms are derived from remnants of an older (probably mid Holocene) marine deposit that was deposited as RSL fell below present MTL (Long et al., 2009). Above 4 cm, the organic silt contains a similar diatom record to that observed on Marsh A2, with oligohalobian-indifferent taxa replaced by oligo- and mesohalobian taxa, notably *Navicula cincta* and *Navicula peregrina.* %LOI is low throughout the sequence and grain size data show the sequence to be a sand-rich silt with a trace of clay. A sample of *Empetrum nigrum* and Cyperaceae seeds and V*accinium* leaves from 4-3 cm depth was dated to 685±35 ^{14}C yr BP (SUERC-16539, 686-559 cal a BP).

A3-3 (Figure 7c)

The stratigraphy is similar to that from A3-6 but here the basal peat is 2 cm thicker. The diatom profile shows that oligoalobhous-indifferent taxa persist throughout the sequence but they

are at their maximum below c. 5 cm where frequencies of *Pinnularia microstauron* and *Pinnularia intermedia* dominate. %LOI data show a decline from >40% between 9-8 cm to <20% above 6 cm. Grain size data show the sediment is a sand with some silt and a trace of clay. Two AMS dates from 7-6 cm and 5-4 cm depth yielded ages of 330±35 ^{14}C yr BP (SUERC-17092, 481-306 cal a BP) and 227±37 ^{14}C yr BP (SUERC-16539, 320-140 cal a BP (78.3% probability)).

5.1.3 Marsh A4

At Marsh A4, high marsh overlies bedrock and passes laterally into freshwater upland environments (Figure 8a). A section through the salt marsh shows a thin, locally preserved grey sand silt above bedrock that passes up into a dark brown humified peat and then into a lighter coloured organic-rich silt sand. The contact between the lower grey silt and the overlying peat undulates with small (cm-scale) ball and flame structures. The sediments above the peat contain occasional sandy laminations and rare angular rock fragments. We analysed five sediment sequences from Marsh A4, two of which are described below (A4-7 and A4-2).

A4-7 (Figure 8b)

The sequence is 7 cm thick and contains a dark brown herbaceous peat overlain by a organic silt sand that extends to the marsh surface. There are high frequencies of *Eunotia praerupta* in the peat, which give way in the overlying sediment to a mixed oligohalobous and mesohalobous assemblage. %LOI is high in the peat (c. 70%) but falls gradually above 5 cm. Grain size data show the post-peat sediment is a sand silt that becomes slightly coarser above 3 cm. A sample of *Empetrum nigrum* seeds and leaves and Cyperaceae seeds from 5-4 cm depth was AMS dated to 208±36 ^{14}C yr BP (SUERC-17081, 310-137 cal a BP (78.2% probability)).

A4-2 (Figure 8c)

The stratigraphy comprises a humified peat overlain at 2 cm by a silt peat that extends to surface. Diatoms are absent through the humified peat but in the silt peat they are dominated by frequencies of *Eunotia praerupta* that decline up profile and are replaced by *Pinnularia microstauron* and then *Nitzschia palea*. %LOI rises through the peat to a maximum of c. 80% at 3-2 cm before falling towards the surface. The sediment above the peat layer is a sand silt. A sample of *Empetrum nigrum* seeds and leaves and Cyperaceae seeds from 1-2 cm depth was AMS dated to 221±36 ^{14}C yr BP (SUERC-17075, 317-140 cal a BP (79.3% probability)).

6. Reconstructing relative sea level

6.1 Transfer function and visual assessment of palaeomarsh surface elevation

The fossil diatom data described above follow a broadly consistent trend, with a lower freshwater peat containing oligohalobous-indifferent taxa that is overlain by salt marsh that has mainly oligo- and mesohalobous taxa. The vertical changes in diatom assemblages are normally gradual and there is no evidence for marsh wide breaks in sedimentation. None of the diatom profiles revert from salt marsh to freshwater upland deposition and none record the establishment of tidal flat environments.

Our transfer function (TF) predicts palaeomarsh elevations for each diatom level counted. The result is 18 records of palaeomarsh elevation that together span the last 600 cal yrs. The overall pattern is for the older freshwater upland environments to be converted into high marsh and in some cases low marsh environments. Sediment accretion is significantly outpaced by the rate of palaeomarsh surface lowering during this initial period of inundation. This is followed by a phase of relatively stable marsh levels that persist through the younger, uppermost levels of most of the studied profiles to the present day. We also use visual assessment (VA) to provide a second estimate of palaeomarsh surface change. We now compare these two approaches for our radiocarbon dated levels (Figure 9) before reconstructing time/altitude trends in RSL. All except one of our reconstructions agree when their vertical ranges are taken into consideration. This gives us confidence that each method of reconstruction is reasonable although there are differences between the results that require consideration.

First, the TF reconstructions generally plot above the equivalent VA estimates for our highest samples (above c. 2.15 m), whereas the reverse is true for samples below this level (Figure 9). This means that overall the TF reconstructions have a wider vertical range (0.89 m) compared to the VA estimates (0.64 m). The cause of these differences lies in the details of each method used. The higher reconstructions of the TF are because the model predicts a relatively high optima for certain key high marsh taxa when compared to the contemporary data, notably *Pinnularia microstauron* (2.30 m MTL) and *Pinnularia borealis* (2.64 m MTL). The latter is above the height at which diatoms are preserved in the contemporary environment (Figure 4). This means that the palaeomarsh elevations of samples containing these species are predicted to be relatively high compared to the equivalent VA reconstructions. Similarly, the lowermost TF reconstructions are sensitive to the presence of *Navicula peregrina* and *Navicula cincta*, each of which have relatively low optima (1.60 m and 1.31 m, respectively) and wide tolerances. For our VA reconstructions we place greater weight on changes in the diatom assemblages that occur around the level of HAT, for example the presence/absence of *Pinnularia microstauron*, *Pinnularia intermedia*, *Nitzschia palea* and *Navicula pusilla*, since these taxa have more tightly defined vertical ranges (Table 2). VA reconstructions are therefore less influenced by the presence of low marsh diatom taxa than the TF method. This is especially evident for the A3-4 (upper) dated level where a mixed assemblage containing high frequencies of *Pinnularia microstauron* and *Navicula*

peregrina generates markedly different predictions of palaeomarsh surface depending on the method used.

Second, the VA reconstructions have a slightly smaller average vertical range compared to those of the TF (± 0.11 m and ± 0.20 m, respectively) (Figure 9). This is because the TF approach considers all the diatom data available in each sample whereas the VA method places greater weight on a smaller number of key taxa that have well defined rises / falls / ranges in the contemporary training set. For example, about the level of HAT (c. 2.33 m), several prominent assemblage changes take place across a vertical range of c. ± 0.10 to 0.15 m (e.g. *Pinnularia microstauron*, *Pinnularia borealis*, *Nitzschia palea*, *Navicula pusilla* (Figure 4)).

Notwithstanding the differences between the two methods the overall trend is similar. Picking which model to use is not easy; the TF method seeks to use all of the diatom data in its reconstructions and is able to easily generate predictions for every sample in a sediment profile, whereas the VA method is more selective in the weight it places on certain taxa and considers trends in adjacent samples. In the following RSL reconstructions we use both methods although our preference is to use the VA method since we believe this better reflects the vertical uncertainties in the contemporary and fossil data used for the reconstructions.

We reject three dates from our analyses because they are modern (SUERC-13888, SUERC-13889, SUERC-17074) and one from A2 Mono 4a (SUERC-13885) which it is clearly inconsistent with the majority of the other bio- and chronostratigraphic data from Marsh A2. We are not able to provide an explanation for the results of these samples which are considerably younger than expected given their elevation and diatom assemblages. Three of the rejected samples contained small quantities of carbon (Table 1) and therefore even small amounts of material not representing the depth under investigation or added during laboratory handling of the sample would have an impact on the radiocarbon result. Radiocarbon analysis of small samples is challenging, but those ≤300µgC indicated in Table 1 were particularly so, requiring AMS analysis at low current (SUERC-13885 and SUERC-13889 contained 240 and 300µgC respectively). It is normal practice to present calibrated radiocarbon ages in age/altitude plots of RSL with a two sigma age range. However, a plateau in the radiocarbon calibration curve means that dates younger than c. AD 1700 have a two sigma probability distribution that extends to present. This renders dates from this time interval of limited value, but alternative dating methods such as ^{210}Pb are also problematic at this time interval. In these cases we cite these dates with a <2 sigma age range (see above). It is important that the resulting RSL plots are considered with this in mind.

6.2 Reconstructing relative sea level change

We combine our chronological and vertical data into two graphs of RSL change (Figure 10). The sample specific vertical errors are determined using a Root Squared Error of the microfossil reconstructions and errors in our levelling and use of tidal datums as defined above. The graphs show the same general pattern with MTL rising from -0.60 ± 0.20 m at c. 600 cal a BP to -0.10 ± 0.20 m at c. 400 cal a BP. After 400 cal a BP, the TF reconstruction suggests RSL may have reached (or was slightly above) 0 m MTL whereas the VA method predicts a stable RSL or slight upwards trend that continued in the last few centuries. By assuming a linear sedimentation rate from the dated levels in the high marsh settings of A4-7 and A3-3, we can utilise TF and VA reconstructions from each centimetre up to the surface (Table 4). This confirms that RSL has been relatively stable for the past 400 years. In Figure 10 we combine our two youngest isolation basin dates from Long et al. (2009) with our salt marsh reconstructions (including eight index points from the recent stable part of the record with inferred ages). This shows that RSL rose from c. – 4 m at c. 1.4 ka cal a BP and reached the present value (within data uncertainty) by 400 cal a BP.

The precision of the new RSL records is considerably better than that associated with the isolation basin method (the latter typically ± 0.40 to 1.0 m (Long et al., 1999)), or the use of radiocarbon dated marine molluscs or archaeological data (typically ± several meters) (Rasch and Jensen, 1997). Our largest source of uncertainty is the radiocarbon chronology. Although we extracted delicate plant macrofossils for dating from 1 cm thick sediment slices, the mean calibrated ages and their associated uncertainties vary by several centuries for samples from a similar elevation. For example, at VA -0.45 m MTL, the two sigma age range of the A2-3 and A3-6 dates span a 400 year interval between c. 700 and 300 cal a BP. The most likely reason for this age scatter is the fact that sediment accretion on these marshes was initially significantly slower than the prevailing rate of RSL rise. The date from A2-4 (540-335 cal a BP, Table 1) formed when VA MTL was c. -0.39 m, however since its formation only 7 cm of salt marsh sediment has accumulated. This means that on these marshes a 1 cm thick slice of sediment probably contains plant macrofossils, especially seeds of *Empetrum nigrum* and Cyperaceae that were deposited over several decades or even centuries.

7. Discussion

7.1 Relative sea level changes in west Greenland during the last millennium

Our new RSL history bears little similarity to either the ‘Th. M.’ or ‘Norse’ models (Figure 2). For example, during the last 400 years both of these models suggest RSL rose by 3 m or so to present, whereas our data show that RSL was within 0.2 m of its present level throughout this interval. At c. AD 1200 both models suggest RSL was c. – 6 m, whereas we identify a late Holocene lowstand of -4 m MTL. Lastly, the ‘Th. M.’ model has a c. 4 m amplitude RSL oscillation

between AD 1200 and AD 1600 but our salt marsh and isolation basin data record a continuous rise throughout; indeed an oscillation of this magnitude would have temporarily converted our highest drowned lake to freshwater, but we see no stratigraphic evidence for this (Long et al., 2009). Our reconstruction shows that RSL reached close to present at c. 400 cal a BP. This is in agreement with Rasch and Nielsen (1995) who argue that sea level in Disko Bugt reached close to present around AD 1500, although we see no evidence for the three 'transgression phases' that they record.

The slow-down in RSL that we observe at c. 400 cal a BP is an important aspect of our results and before we discuss this further we now consider whether this is real or an artefact of our data processing. One possibility is that our vertical reconstructions are incorrect, perhaps because they over- or under-estimate the actual tide level; we think this unlikely since they are made using extensive contemporary and fossil data and two different reconstruction methods. Uncertainties in tidal datums and survey methods do not explain the trends observed, since we use the same datums for our modern and fossil analyses. Our study sites are small marshes in a fjord setting, close to the open coast, and there is no reason why abrupt decimeter changes in palaeotidal range should have occurred at 400 cal a BP. Lastly, we have considered whether the radiocarbon ages are unreliable, but we think this unlikely since we use the same sampling approach and materials throughout our analyses (terrestrial macrofossils). In summary, we have confidence in our reconstructions and believe that the slow-down in RSL at c. 400 cal a BP is real. We suggest that the large differences between our reconstructions and those of Weidick (1993) (Figure 2) most likely reflect the problems in relating archaeological data to former tidal datums, as well as the uncertainties that arise when compiling data from a large area that has likely recorded different rates of RSL change.

7.2 Driving mechanisms of relative sea level

Relative sea level at Sisimiut, as elsewhere in Greenland, is controlled by a combination of non-Greenland and Greenland processes. The former include changes in eustasy and the elevation of the solid earth due to the collapse of the forebulge associated with non-local ice sheet deglaciation (Fleming and Lambeck, 2004). The latter arises from rebound due to the unloading of Greenland ice since the LGM as well as a potential reloading of the solid earth during the neoglacial (e.g. Kelly, 1980). We now explore these contributions as we consider the driving mechanisms behind RSL change at the study site.

7.2.1 Non-Greenland processes

The collapse of the Laurentide forebulge is an important control on late Holocene RSL in west Greenland. Fleming and Lambeck (2004) estimate that since 2 k a ^{14}C BP (c. 1.8 k cal a BP) this has caused ~13 m of RSL rise at Sisimiut, at an average rate of c. 7 mm yr. By comparison, the ICE-5G model (Peltier, 2004) predicts a non-Greenland contribution to RSL rise at Sisimiut of c. 4.5 m since 1 k cal a BP, at an average rate of 4.5 mm yr (Simpson et al., 2009). These two models, which have different earth and ice model parameters, provide a range of estimates (7 to 4.5 mm yr) for the non-Greenland solid earth contribution during the last few millennia. The collapse of the Laurentide forebulge is a slow, gradual process driven by the viscoelastic response of the Earth's crust to ice unloading following the end of the Late Wisconsnian. Although rates of forebulge collapse gradually reduce over the Holocene, there is no reason why they should slow or stop, which would be required to cause the slow-down in RSL we observe at 400 cal a BP.

It is unlikely that the Sisimiut RSL record contains a significant contribution from 'eustatic' sea level change. This is because the overall rise of c. 4 m since 1.4 k cal a BP far exceeds most estimates of the eustatic contribution during this period. Most studies indicate that there was zero eustatic contribution to global sea level change to within observational uncertainty (e.g. Lambeck, 2002; Peltier, 2004; Milne et al., 2005). With regard to the RSL slow-down observed at 400 cal a BP, a eustatic fall of similar magnitude to the rise driven by peripheral bulge subsidence would be required (i.e. several mm/yr). Such a signal, which would amount to a metre or more fall in global sea level over the past 400 years, has not been observed. We conclude that, while there most likely have been fluctuations in eustatic sea level over the past millennium (e.g. Grinsted et al., 2009), they have been limited to a few decimetres in amplitude and so are not a primary control of the changes observed at Sisimiut.

In summary, although non-Greenland processes, particularly the collapse of the Laurentide forebulge, are significant in controlling RSL in the study area, they cannot explain the slow-down and then near-stable RSL observed from c. 400 cal a BP onwards. For this reason, we now turn attention to consider local, Greenland processes.

7.2.2 Local (Greenland) processes

The significant removal of ice load from west Greenland since the last glacial maximum caused glacio-isostatic rebound that in west Greenland exceeded other non-Greenland processes for most of the Holocene. The physical manifestation of this interplay is the elevation of the marine limit (the highest level reached by the sea following ice margin retreat) which in the study area is at c. 120 m asl (Funder, 1989). The solid Earth response to Greenland ice unloading decreased during the Holocene and caused the rate of Greenland rebound and RSL fall to gradually slow. Ice sheet models suggest that the neoglacial expansion of the ice sheet added new load and further

reduced the rate of Greenland rebound, such that non-Greenland (largely Laurentide forebulge collapse) subsidence started to dominate and RSL rose (e.g. Simpson et al., 2009).

This interplay of non-Greenland and Greenland processes can reasonably explain most of the features of the Holocene RSL history of the study area. However, the RSL slow-down at c. 400 cal a BP is more difficult to explain since, if our arguments above regarding non-Greenland processes are valid, we require a local Greenland process to contribute a sustained decrease in RSL between 400 cal a BP and the present that is equal in magnitude to other, non-Greenland processes. This would require a local or regional mass loss during a period that encompasses the latter part of the Little Ice Age when, as we note above, many glaciers and ice caps in Greenland and elsewhere are thought to have been at their maximum late neoglacial size (although we note that there is uncertainty in the date at which the ice sheet first reached its maximum extent in many areas (Weidick, 1968)).

It is not immediately obvious how this region of west Greenland could lose mass during the Little Ice Age. We know from a variety of sources that the Little Ice Age was a period of pronounced climate variability in Greenland and the North Atlantic region more widely which was more complex than a simple shift to colder conditions (Barlow, 2001). Recent studies of the mass balance of the Greenland ice sheet show its sensitivity to various climate forcings including the North Atlantic Oscillation (NAO) (Hanna et al., 2008) and it is interesting to note that Trouet et al. (2009) suggest a persistent shift from a strongly positive to a negative NAO state before and after AD 1400-1600. It is reasonable to hypothesise that changes of this type would have had a significant impact on the Greenland Ice Sheet and hence RSL change through changes in both its surface mass balance and glacier dynamics.

Recent observations of the Greenland Ice Sheet demonstrate its sensitivity to changes in the behaviour of its major ice streams (e.g. Luthcke et al., 2006). The Jakobshavn ice stream drains a large part of the west Greenland ice sheet and we note that Lloyd (2006) observes an increase in sedimentation rate, ice rafted debris and a change in foraminifera assemblages from c. 500 cal a BP in a sea bed sediment core from Disko Bugt. These changes could reflect an increase in discharge from Jakobshavn that might have contributed to a regional reduction in ice load. Another potential mechanism involves a shift to regional negative mass balance due to the cold and dry conditions, with low precipitation, that prevailed in this part of west Greenland around this time. For example, a recent study of lake levels in the Søndre Strømfjord area shows that they fell to their lowest Holocene level during the Little Ice Age (Aebly and Fritz, 2009). A further possibility is that the RSL slow-down records a delayed response to earlier events in the ice sheet's history (Huybrechts, 1994), including the warmth of the proceeding medieval warm period

when the ice sheet may have lost mass (Dahl-Jensen et al., 1998). Clearly, these hypotheses require testing with suitable ice and sea-level models to ascertain their validity.

The above discussion shows that we do not yet understand the cause of the recent slow-down in RSL observed at our field site. This may be remedied by a better understanding of the physics of ice streams and development of more sophisticated ice models that accurately describe changes in ice discharge. We believe that our reconstruction is robust, since it is based on multiple sediment profiles examined from several marshes and using two methods of reconstruction. We note that the evidence for relatively stable RSL at present is similar to the trend recorded in recent repeat GPS measurements at Sisimiut (Dietrich et al., 2005). Moreover, work elsewhere in Disko Bugt also suggests that RSL reached close to present in the fifteenth century (Rasch and Nielsen, 1995). Preliminary results from a comparable salt marsh based study in outer Disko Bugt also indicate that a RSL slow-down c. 400 cal a BP occurred in this region (Woodroffe and Long, 2009b). This change in recent RSL appears to be a regional-scale event and not simply the product of local site processes.

8. Conclusions

We present the results of a detailed investigation into the pattern of relative sea level (RSL) changes at a field site located close to Sisimiut, west Greenland. Our approach uses a combination of litho-, bio- and chronostratigraphic methods to reconstruct RSL change in the last millennium using salt marsh sediments. This is the first systematic analysis of this type in Greenland and demonstrates the potential of the methods used in these and potentially other high latitude salt marshes. The conclusions from this study are as follows:

1. The stratigraphy of the salt marshes in the study area record an upwards transition from freshwater to salt marsh conditions during the last 800 years or so. This change in palaeomarsh elevation is recorded in thin sediment sections, typically 5 to 10 cm thick, that in most instances overlie bedrock.

2. We use a diatom-based transfer function (TF) to reconstruct palaeomarsh elevation and changes in mean tide level (MTL) using a dataset previously published by Woodroffe and Long (2009a). We also use visual assessment (VA) that takes into account vertical trends in the diatom data as well as the sedimentological information to provide a second set of reconstructions.

3. Both TF and VA approaches yield similar results, giving us confidence in each. In general, MTL rose from c. -0.60 ± 0.20 m at c. 600 cal a BP to reach -0.10 ± 0.20 m at c. 400 cal a BP. After this time, MTL remained close to present (± 0.20 m) until the present day. The range of the TF

reconstructions is larger than the VA reconstructions, reflecting the fact that the TF is sensitive to the optima and tolerances of taxa that occur at the upper and lower end of the contemporary training set. The VA model has generally smaller height uncertainties because of its reliance on certain key changes in diatom taxa that occur at well defined levels in the intertidal zone.

4. Our new record demonstrates that existing models of RSL change that invoke meter scale oscillations in RSL since AD 1600 are not valid in this sector of west Greenland. Although RSL was rising during the final centuries of the Norse period, after c. AD 1600 RSL had been close to present.

5. The initial rise in late Holocene RSL can be explained by the dominance of non-Greenland processes, notably the collapse of the Laurentide forebulge, over local (Greenland) solid Earth uplift associated with postglacial ice unloading. The slow-down in RSL at 400 cal a BP is unlikely to record either a change in the rate of Laurentide forebulge collapse or a change in eustatic sea level. We therefore argue that this change reflects a sustained reduction in local (Greenland) ice mass, the impact of which persists over most of the past 400 years.

6. The last 400 years is widely acknowledged as a period of generally cooler than present conditions associated with the latter stages of the Little Ice Age. During this period, existing models suggest that the ice expanded to its maximum extent. It is not obvious at this stage how to reconcile an expanding ice sheet with a reduction in ice load.

Acknowledgements

We thank Will Todd and for his help in the field, Katie Stokes for help in the laboratory, and Palle Bo Nielsen and Kisser Thorsøe for advice regarding tidal matters. The research was completed as part of NERC Grant NE/C519311/1. We thank the NERC Radiocarbon Laboratory and SUERC AMS Laboratory in East Kilbride, Scotland for support with the radiocarbon dating under award number 1234.0407 and in particular the meticulous work of Tanya Ertunc and Sheng Xu. We thank two referees for their constructive comments on this paper, which is a contribution to IGCP 495 project “Quaternary land-ocean interactions: driving mechanisms and coastal responses” and to the INQUA Commission on Coastal and Marine Processes.

Supplementary data

In this supplementary information we provide details of the lithology, diatoms and radiocarbon dates from the salt marsh samples not detailed in the main paper. These are from: Marsh 2 (A2-3, A2-Mono 4A and A2 Mono 7, Figures SI1a-c), Marsh 3 (A3-1 and A3-4, Figures SI2

a, b) and Marsh 4 (A4-1, A4-5, A4-6 and A4-9, Figures SI3 a-d). In each diagram counts are expressed as a percentage of total diatom valves (%TDV) and only data >5% TDV are shown. Radiocarbon dates are listed in full in Table 1 of the main paper.

References

Aebly, F.A., Fritz, S.C., 2009. Palaeohydrology of Kangerlussuaq (Sondre Stromfjord), West Greenland during the last ~8000 years. Holocene 19 (1), 91-104.

Barlow, L.K., 2001. The time period AD 1400-1900 in Central Greenland ice cores in relation to the North Atlantic sector. Climatic Change 48, 101-119.

Bronk Ramsey, C., 2001. Development of the radiocarbon calibration program. Radiocarbon 43 (2 A), 355-363.

Bronk Ramsey, C., 1995. Radiocarbon calibration and analysis of stratigraphy: the OxCal program. Radiocarbon 37 (2), 425-430.

Craig, H., 1957. Isotopic standards for carbon and oxygen and correction factors for mass-spectrometric analysis of carbon dioxide. Geochimica et Cosmochimica Acta 12, 133-149.

Dahl-Jensen, D., Mosegaard, K., Gundestrup, N., Clow, G.D., Johnsen, S.J., Hansen, A.W., Balling, N., 1998. Past temperatures directly from the Greenland Ice Sheet. Science 282, 268-271.

Dietrich, R., Rulke, A., Scheinert, M., 2005. Present-day vertical crustal deformations in West Greenland from repeated GPS observations. Geophysical Journal International 163 (3), 865-874.

Fleming, K., Lambeck, K., 2004. Constraints on the Greenland Ice Sheet since the Last Glacial Maximum from sea-level observations and glacial-rebound models. Quaternary Science Reviews 23 (9-10), 1053-1077.

Funder, S., 1989. Quaterary geology of the ice free areas and adjacent shelves of Greenland. In: R.J. Fulton (Editor), Quaternary Geology of Canada and Greenland. Geology of Canada 1, Geological Society of Canada, Ottawa, pp. 743-792.

Gabel-Jørgensen, C.C.A., Egedal, J., 1940. Tidal observations made at Nanortalik and Julianehåb in 1932-34. Meddelelser om Grønland 107 (2), 1-47.

Gehrels, W.R., Marshall, W.A., Gehrels, M.J., Larsen, G., Kirby, J.R., Eriksson, J., Heinemeier, J., Shimmield, T., 2006. Rapid sea-level rise in the North Atlantic Ocean since the first half of the 19th century. The Holocene 16, 948-964.

Grinsted, A., Moore, J.C., Jevrejeva, S., 2009. Reconstructing sea level from palaeo and projected temperatures 200 to 2100 AD. Climate Dynamics doi:10.1007/s00382-008-0507-2.

Hanna, E., Huybrechts, P., Steffen, K., Cappelen, J., Huff, R., Shuman, C., Irvine-Fynn, T., Wise, S., Griffiths, M., 2008. Increased runoff from melt from the Greenland Ice Sheet: A response to global warming. Journal of Climate 21 (2), 331-341.

Heiri, O., Lotter, A.F., Lemcke, G., 2001. Loss on ignition as a method for estimating organic and carbonate content in sediments: Reproducibility and comparability of results. Journal of Paleolimnology 25 (1), 101-110.

Huybrechts, P., 1994. The present evolution of the Greenland Ice-Sheet - an assessment by modelling. Global and Planetary Change 9 (1-2), 39-51.

Kelly, M., 1980. The status of the Neoglacial in Western Greenland. Rapport Grønlands Geologiske Undersøgelse 96, 1-24.

Lambeck, K., 2002. Sea level change from mid Holocene to recent time: an Australian example with global implications. In: J.X. Mitrovica and B.L.A. Vermeersen (Editors), Ice Sheets, Sea Level and the Dynamic Earth, Geodynamics Series 29. American Geophysical Union, pp. 33-50.

Lepping, O., Daniëls, F.J.A., 2007. Phytosociology of beach and salt marsh vegetation in northern West Greenland. Polarforschung 76 (3), 95-108.

Lloyd, J.M., 2006. Late Holocene environmental change in Disko Bugt, West Greenland: interaction between climate, ocean circulation and Jakobshavn Isbrae. Boreas 35 (1), 35-49.

Long, A.J., Roberts, D.H., Rasch, M., 2003. New observations on the relative sea level and deglacial history of Greenland from Innaarsuit, Disko Bugt. Quaternary Research 60 (2), 162-171.

Long, A.J., Roberts, D.H., Wright, M.R., 1999. Isolation basin stratigraphy and Holocene relative sea-level change on Arveprinsen Ejland, Disko Bugt, West Greenland. Journal of Quaternary Science 14 (4), 323-345.

Long, A.J., Woodroffe, S.A., Dawson, S., Roberts, D.H., Bryant, C.L., 2009. Late Holocene relative sea-level rise and the Neoglacial history of the Greenland ice sheet. Journal of Quaternary Science 24 (4), 345-359.

Luthcke, S.B., Zwally, H.J., Abdalati, W., Rowlands, D.D., Ray, R.D., Nerem, R.S., Lemoine, F.G., McCarthy, J.J.,Chinn, D.S., 2006. Recent Greenland ice mass loss by drainage system from satellite gravity observations. Science 314 (5803), 1286-1289.

Mikkelsen, N., Kuijpers, A., Arneborg, J., 2008. The Norse in Greenland and late Holocene sea-level change. Polar Record 44 (228), 45-50.

Milne, G.A., Long, A.J.,Bassett, S.E., 2005. Modelling Holocene relative sea-level observations from the Caribbean and South America. Quaternary Science Reviews 24, 1183-1202.

Palmer, A.J.M.,Abbott, W.H., 1986. Diatoms as indicators of sea-level change. In: O. Van De Plassche (Editor), Sea-level research. Geo Books, Norwich, pp. 457-487.

Peltier, W.R., 2004. Global glacial isostasy and the surface of the ice-age earth: The ICE-5G (VM2) model and GRACE. Annual Review of Earth and Planetary Sciences 32, 111-149.

Porter, S.C., 2000. Onset of neoglaciation in the Southern Hemisphere. Journal of Quaternary Science 15 (4), 395-408.

Rasch, M., 2000. Holocene relative sea level changes in Disko Bugt, West Greenland. Journal of Coastal Research 16 (2), 306-315.

Rasch, M., Jensen, J.F., 1997. Ancient Eskimo dwelling sites and Holocene relative sea-level changes in southern Disko Bugt, central West Greenland. Polar Research 16 (2), 101-115.

Rasch, M., Nielsen, N., 1995. Coastal morpho-stratigraphy and Holocene relative sea level changes at Tuapaat, southeastern Disko Island, central West Greenland. Polar Research 14 (3), 277-289.

Simpson, M.J.R., Milne, G.A., Huybrechts, P.,Long, A.J., 2009. Calibrating a glaciological model of the Greenland ice sheet from the last glacial maximum to present-day using field observations of relative sea level and ice extent. Quaternary Science Reviews 28, 1631-1657.

Sparrenbom, C.J., Bennike, O., Björck, S., Lambeck, K., 2006. Relative sea-level changes since 15 000 cal. yr BP in the Nanortalik area, Southern Greenland. Journal of Quaternary Science 21 (1), 29-48.

Trouet, V., Esper, J., Graham, N.E., Baker, A., Scourse, J.D., Frank, D.C., 2009. Persistent positive North Atlantic Oscillation mode dominated the Medieval Climate Anomaly. Science 324 (5923), 78-80.

van Tatenhove, F.G.M., Olesen, O.B., 1994. Ground temperature and related permafrost characteristics in West Greenland. Permafrost and Periglacial Processes 5, 199-215.

Wanner, H., Beer, J., Butikofer, J., Crowley, T.J., Cubasch, U., Fluckiger, J., Goosse, H., Grosjean, M., Joos, F., Kaplan, J.O., Kuttel, M., Muller, S.A., Prentice, I.C., Solomina, O., Stocker, T.F., Tarasov, P., Wagner, M., Widmann, M., 2008. Mid- to Late Holocene climate change: an overview. Quaternary Science Reviews 27 (19-20), 1791-1828.

Weidick, A., 1993. Neoglacial change of ice cover and the related response of the Earth's crust in West Greenland. Rapport Grønlands Geologiske Undersøgelse 159, 121-126.

Weidick, A., 1968. Observations on some Holocene glacier fluctuations in West Greenland. Grønlands Geologiske Undersøgelse Bulletin, 165, 202 pp.

Woodroffe, S.A., Long, A.J., 2009a. Salt marshes as archives of recent relative sea-level change in West Greenland. Quaternary Science Reviews 28, 1750-1761.

Woodroffe, S.A., Long, A.J., 2009b. Reconstructing recent relative sea-level changes in West Greenland: local diatom-based transfer functions are superior to regional models. Quaternary International doi:10.1016/j.quaint.2009.06.005.

List of Figures

basin data from Long et al. (2009). Open squares (A4-7) and diamonds (A3-3) denote reconstructions with inferred ages assuming constant sedimentation rates between the surface and the ^{14}C date in that sequence. Solid squares are the youngest isolation basin data from Long et al. (2009). Height and age errors are defined in Tables 2 and 4. Age errors for the diatom levels from A4-7 and A3-3 are estimated based on the assumption that they decrease linearly to present.

Supplementary information

In this supplementary information we provide details of the lithology, diatoms and radiocarbon dates from the salt marsh samples not detailed in the main paper. These are from: Marsh 2 (A2-3, A2-Mono 4A and A2 Mono 7, Figures SI1a-c), Marsh 3 (A3-1 and A3-4, Figures SI2 a, b) and Marsh 4 (A4-1, A4-5, A4-6 and A4-9, Figures SI3 a-d). In each diagram counts are expressed as a percentage of total diatom valves (%TDV) and only data >5% TDV are shown. Radiocarbon dates are listed in full in the main paper.

Table 1 Radiocarbon dates from the study area. $\delta^{13}C$ values were measured using a dual-inlet mass spectrometer with a multiple ion beam collection facility (VG OPTIMA) for correcting ^{14}C data to –25 ‰ $\delta^{13}C_{VPDB}$. Starred $\delta^{13}C$ values indicate samples containing ≤300µg C, which required AMS analysis at low current. The starred $\delta^{13}C$ values were calculated from $\delta^{13}C/^{12}C$ ratios measured during AMS ^{14}C determination and by comparison to Craig (1957) $\delta^{13}C/^{12}C$ values for PDB. These values are not necessarily representative of the $\delta^{13}C$ in the original sample material. $\delta^{13}C$ values with pluses were estimated, as there was insufficient material for direct measurements.

Sample code and depth below surface (cm)	**Laboratory code**	**Material dated**	**Sample elevation (m MTL)**	**Sample weight (mg)**	**$\delta^{13}C_{VPDB}$ ‰ ± 0.1**	**Conventional radiocarbon age (years BP ± 1 σ)**	**Age range (cal. yrs BP, ± 2 σ)**	**Age range (cal. yrs AD, ± 2 σ)**
Marsh A2								
A2-3 (6-7 cm)	SUERC-13884	*Empetrum nigrum* seeds and leaves and Cyperaceae seeds	1.56	3.78	-24.4*	397 ± 47	540-316	1410-1634
A2-4 (7-8 cm)	SUERC-46540	*Empetrum nigrum* seeds and leaves and Cyperaceae seeds	1.46	1.00	-28.1*	445 ± 35	540-335	1410-1615
A2 Mono 4a (11-12 cm)	SUERC-13885	Cyperaceae seeds	1.36	3.70	-26.3*	161 ± 47	289-0	1661-1950
A2 Mono 6 (9-10 cm)	SUERC-13886	*Empetrum nigrum* seeds and leaves and Cyperaceae seeds	1.28	3.49	-26.5*	640 ± 48	662-559	1288-1391
A2 Mono 7 (12-14 cm)	SUERC-13887	*Empetrum nigrum* seeds and leaves and Cyperaceae seeds	0.97	1.03	-24.8*	587 ± 48	658-528	1292-1422
A2 Mono 7 (12-13 cm)	SUERC-13888	*Vaccinium uliginosum* leaf	0.97	1.44	-23.8*	Modern	n/a	n/a
A2 Mono 7 (13-14 cm)	SUERC-13889	Piece of lichen (?)	0.97	3.32	-22.2*	Modern	n/a	n/a
Marsh A3								
A3-1 Lower (9-10 cm)	SUERC-17091	Cyperaceae seeds, *Empetrum nigrum* seeds and leaves and	1.99	2.96	-27.1	346 ± 36	490-311	1460-1639

Sample code and depth below surface (cm)	Laboratory code	Material dated	Sample elevation (m MTL)	Sample weight (mg)	$\delta^{13}C_{VPDB}$ ‰ ± 0.1	Conventional radiocarbon age (years BP ± 1 σ)	Age range (cal. yrs BP, ± 2 σ)	Age range (cal. yrs AD, ± 2 σ)
		Vaccinium uliginosum leaves						
A3-1 Upper (6-7 cm)	SUERC-20016	Cyperaceae and *Empetrum nigrum* seeds and *Vaccinium uliginosum* leaves	2.02	1.26	-27.9*	395 ± 35	540-316	1410-1634
A3-3 Lower (6-7 cm)	SUERC-17092	*Empetrum nigrum* seeds and leaves and Cyperaceae seeds	1.87	7.30	-26.0	330 ± 35	481-306	1469-1644
A3-3 Upper (4-5 cm)	SUERC-19489	*Empetrum nigrum* seeds and *Vaccinium uliginosum* leaves	1.89	4.44	-24.3^{+}	227 ± 37	426-0	1630-1950
A3-4 Lower (8-9 cm)	SUERC-17096	*Empetrum nigrum* seeds and leaves	1.84	4.30	-24.6	669 ± 36	680-556	1270-1394
A3-4 Upper (6-7 cm)	SUERC-17097	*Empetrum nigrum* seeds and leaves	1.86	1.44	-28.6*	355 ± 35	497-315	1453-1635
A3-6 (3-4 cm)	SUERC-16539	Cyperaceae and *Empetrum nigrum* seeds and *Vaccinium uliginosum* leaves	1.73	2.70	-38.6*	685 ± 35	686-559	1264-1391
Marsh A4								
A4-1 (2-3 cm)	SUERC-17074	Cyperaceae and *Empetrum nigrum* seeds and *Harrimanella hypnoides* leaves	2.48	1.50	-27.9	Modern	n/a	n/a
A4-2 (1-2 cm)	SUERC-17075	Cyperaceae and *Empetrum nigrum* seeds and *Vaccinium uliginosum* leaves	2.42	7.50	-26.7	221 ± 36	422-0	1633-1950
A4-5 (1-2 cm)	SUERC-16538	*Empetrum nigrum* seeds and leaves and Cyperaceae seeds	2.28	12.90	-49.5*	385 ± 35	510-371	1440-1633

Sample code and depth below surface (cm)	Calibrated age range (BP +/- 2 σ unless specified)	Sample elevation (m MTL)	Palaeomarsh surface elevation (m MTL) Transfer Function	Palaeomarsh surface elevation (m MTL) Visual Assessment	RSL reconstruction (m MTL) Transfer Function	RSL reconstruction (m MTL) Visual Assessment	MinDC (87.77 = largest in modern training set)	Accept or reject reconstruction

Sample code and depth below surface (cm)	Laboratory code	Material dated	Sample elevation (m MTL)	Sample weight (mg)	$\delta^{13}C_{VPDB}$ ‰ ± 0.1	Conventional radiocarbon age (years BP ± 1 σ)	Age range (cal. yrs BP, ± 2 σ)	Age range (cal. yrs AD, ± 2 σ)
A4-6 (3-4 cm)	SUERC-17080	*Empetrum nigrum* seeds and leaves and Cyperaceae seeds	2.23	1.50	-26.0	265 ± 36	459-0	1491-1950
A4-7 (4-5 cm)	SUERC-17081	*Empetrum nigrum* seeds and leaves and Cyperaceae seeds	2.18	1.00	-26.5	208 ± 36	310-0	1640-1950
A4-9 (4-5 cm)	SUERC-17085	*Empetrum nigrum* seeds and leaves and Cyperaceae seeds	2.08	1.00	-27.5	281 ± 36	460-0	1490-1950
A4-10 (3-4 cm)	SUERC-17086	*Empetrum nigrum* seeds and leaves and Cyperaceae seeds	2.03	1.00	-27.4	354 ± 36	497-315	1453-1635

Table 2 Reconstructed palaeomarsh surface elevation and relative sea level data from the study area using the transfer function (TF) and visual assessment (VA) methods. TF and VA palaeomarsh surface elevation errors are equal to the RMSEP and the ranges of the species detailed in Table 3 and 4 respectively. The RSL errors include all uncertainties in the reconstructions and are those used in Figure 10. The minimum dissimilarity coefficient (Min DC) value is a measure within the modern analogue technique that provides an indication of how reliable the TF reconstructions are.

Marsh A2								
A2-3 (6-7 cm)	540-316	1.56	2.09 ± 0.19	2.17 ± 0.12	-0.53 ± 0.20	-0.61 ± 0.13	57.91	Accept
A2-4 (7-8 cm)	540-335	1.46	1.50 ± 0.19	1.85 ± 0.17	-0.04 ± 0.19	-0.39 ± 0.18	27.86	Accept
A2 Mono 4a (11-12 cm)	289-0	1.36	1.62 ± 0.15	1.81 ± 0.14	-0.25 ± 0.16	-0.45 ± 0.15	102.09	Reject
A2 Mono 6 (9-10 cm)	662-559	1.28	2.15 ± 0.20	2.13 ± 0.16	-0.88 ± 0.20	-0.85 ± 0.16	93.05	Accept
A2 Mono 7 (12-14 cm)	658-528	0.97	1.49 ± 0.20	1.84 ± 0.14	-0.52 ± 0.21	-0.85 ± 0.15	58.53	Accept
Marsh A3								
A3-1 Lower (9-10 cm)	490-311	1.99	2.38 ± 0.20	2.22 ± 0.07	-0.39 ± 0.21	-0.24 ± 0.08	50.27	Accept
A3-1 Upper (6-7 cm)	540-316	2.01	1.87 ± 0.22	2.01 ± 0.04	0.15 ± 0.22	0.00 ± 0.07	27.71	Accept
A3-3 Lower (6-7 cm)	481-306	1.87	2.30 ± 0.20	2.13 ± 0.16	-0.43 ± 0.21	-0.26 ± 0.16	48.07	Accept
A3-3 Upper (4-5 cm)	320-140 (78.3 %)	1.89	1.83 ± 0.20	1.99 ± 0.06	0.06 ± 0.21	-0.10 ± 0.08	104.30	Accept
A3-4 Lower (8-9 cm)	680-556	1.84	2.27 ± 0.19	2.13 ± 0.16	-0.43 ± 0.19	-0.29 ± 0.16	31.50	Accept
A3-4 Upper (6-7 cm)	497-315	1.86	1.79 ± 0.19	2.01 ± 0.06	0.07 ± 0.19	-0.14 ± 0.08	48.07	Accept
A3-6 (3-4 cm)	686-559	1.73	1.89 ± 0.22	2.07 ± 0.12	-0.16 ± 0.23	-0.34 ± 0.13	14.69	Accept
Marsh A4								
A4-1 (2-3 cm)	Modern	2.48	2.30 ± 0.20	2.49 ± 0.12	0.15 ± 0.21	-0.01 ± 0.13	70.85	Reject
A4-2 (1-2 cm)	317-140 (79.3 %)	2.42	2.32 ± .0.19	2.45 ± 0.12	0.10 ± 0.20	-0.03 ± 0.13	62.67	Accept
A4-5 (1-2 cm)	510-371	2.28	2.31 ± 0.19	2.30 ± 0.11	-0.03 ± 0.19	-0.02 ± 0.12	24.53	Accept
A4-6 (3-4 cm)	459-275 (83.1 %)	2.23	2.27 ± 0.18	2.23 ± 0.06	-0.04 ± 0.19	0.00 ± 0.08	25.37	Accept

Sample number and depth below surface (cm)	Sample elevation (m MTL)	Visual Assessment reconstruction criteria (range refers to presence of diatom species above 5 % TDV)	Palaeomarsh surface elevation (m MTL)	RSL reconstruction (m MTL)	Visual Assessment method
Marsh A2					
A2-3 (6-7 cm)	1.56	*Pinnularia microstauron* rising (2.29-1.95 m MTL range) *Pinnularia intermedia* falling (2.61-2.06 m MTL range)	2.17 ± 0.12	-0.61 ± 0.13	
A2-4	1.46	*Navicula cincta* rising (rises to peak of 55 % TDV at 1.68 m	1.85 ± 0.17	-0.39 ± 0.18	
A4-7 (4-5 cm)	310-137 (78.2 %)	2.18	2.26 ± 0.20	2.27 ± 0.15	-0.08 ± 0.21	0.09 ± 0.16	39.12	Accept
A4-9 (4-5 cm)	460-283 (92 %)	2.08	2.32 ± 0.19	2.17 ± 0.12	0.24 ± 0.20	0.09 ± 0.13	53.00	Accept
A4-10 (3-4 cm)	497-315	2.03	2.26 ± 0.19	2.09 ± 0.10	-0.23 ± 0.20	0.06 ± 0.11	54.42	Accept

Table 3 Visual Assessment reconstruction criteria for reconstructing palaeomarsh surface elevation and relative sea level. The elevation estimates derived for the RSL reconstructions include these errors and all other sampling errors described in the text.

(7-8 cm)		MTL, with first occurrence >5 % TDV at 2.02 m MTL) *Caloneis borealis* present (2.19-1.44 m MTL range)		
A2 Mono 4a (11-12 cm)	1.36	*Pinnularia microstauron* absent (2.29-1.95 m MTL range) *Pinnularia intermedia* absent (2.61-2.06 m MTL range) *Navicula cincta* rising (rises to peak of 55 % TDV at 1.68 m MTL, with first occurrence >5 % TDV at 2.02 m MTL)	1.81 ± 0.14	-0.45 ± 0.15
A2 Mono 6 (9-10 cm)	1.28	*Pinnularia microstauron* falling (2.29-1.95 m MTL range) *Navicula pusilla* present (2.42-1.98 m MTL range)	2.13 ± 0.16	-0.85 ± 0.16
A2 Mono 7 (12-14 cm)	0.97	*Pinnularia microstauron* absent (2.29-1.95 m MTL range) *Pinnularia intermedia* absent (2.61-2.06 m MTL range) *Navicula cincta* rising (rises to peak of 55 % TDV at 1.68 m MTL, with first occurrence >5 % TDV at 2.02 m MTL)	1.84 ± 0.14	-0.85 ± 0.15
Marsh A3				
A3-1 Lower (9-10 cm)	1.99	*Pinnularia microstauron* rising (2.29-1.95 m MTL range) *Pinnularia intermedia* falling (2.61-2.06 m MTL range) *Luticola mutica* present (2.41-2.16 m MTL range)	2.22 ± 0.07	-0.24 ± 0.08
A3-1 Upper (6-7 cm)	2.01	*Pinnularia microstauron* falling (2.29-1.95 m MTL range) *Navicula pusilla* present (2.42-1.98 m MTL range) *Pinnularia intermedia* fallen below 5 % (2.61-2.06 m MTL range)	2.01 ± 0.04	0.00 ± 0.07
A3-3 Lower (6-7 cm)	1.87	*Pinnularia intermedia* falling (2.61-2.06 m MTL range) *Pinnularia microstauron* rising (2.29-1.95 m MTL range) *Navicula pusilla* present (2.42-1.98 m MTL range)	2.13 ± 0.16	-0.26 ± 0.16
A3-3 Upper (4-5 cm)	1.89	*Pinnularia microstauron* falling (2.29-1.95 m MTL range) *Pinnularia intermedia* absent (2.61-2.06 m MTL range)	1.99 ± 0.06	-0.10 ± 0.08
A3-4 Lower (8-9 cm)	1.84	*Pinnularia intermedia* present (2.61-2.06 m MTL range) *Pinnularia microstauron* rising (2.29-1.95 m MTL range) *Navicula pusilla* present (2.42-1.98 m MTL range) *Luticola mutica* present (2.41-2.16 m MTL range)	2.13 ± 0.16	-0.29 ± 0.16
A3-4 Upper (6-7 cm)	1.86	*Pinnularia intermedia* absent (2.61-2.06 m MTL range) *Pinnularia microstauron* falling (2.29-1.95 m MTL range) *Navicula pusilla* absent (2.42-1.98 m MTL range) *Nitzschia palea* absent (2.41-1.84 m MTL range)	2.01 ± 0.06	-0.14 ± 0.08
A3-6 (3-4 cm)	1.73	*Pinnularia microstauron* falling (2.29-1.95 m MTL range) *Pinnularia intermedia* absent (2.61-2.06 m MTL range) *Caloneis borealis* present (2.19-1.44 m MTL range)	2.07 ± 0.12	-0.34 ± 0.13
Marsh A4				
A4-1 (2-3 cm)	2.48	*Eunotia praerupta* falling (2.57-2.34 m MTL range) *Pinnularia microstauron* present (2.29-1.95 m MTL range) *Pinnularia intermedia* rising (2.61-2.06 m MTL range)	2.49 ± 0.12	-0.01 ± 0.13

Sample code and depth below surface (cm)	Sample elevation (m MTL)	Visual Assessment reconstruction criteria (range refers to presence of diatom species above 5 % TDV)	Palaeomarsh surface elevation (m MTL) Visual Assessment	RSL (m MTL) Visual Assessment	Palaeomarsh surface elevation (m MTL) Transfer Function	RSL (m MTL) Transfer Function
A4-2 (1-2 cm)	2.42	*Navicula pusilla* present (2.42-1.98 m MTL range) *Eunotia praerupta* falling (2.57-2.34 m MTL range)		2.45 ± 0.12	-0.03 ± 0.13	
A4-5 (1-2 cm)	2.28	*Eunotia praerupta* rising (2.57-2.34 m MTL range) *Pinnularia intermedia* falling (2.61-2.06 m MTL range) *Nitzschia palea* present (2.41-1.84 m MTL range)		2.30 ± 0.11	-0.02 ± 0.12	
A4-6 (3-4 cm)	2.23	*Pinnularia intermedia* rising (2.61-2.06 m MTL range) *Pinnularia microstauron* present (2.29-1.95 m MTL range) *Nitzschia palea* present (2.41-1.84 m MTL range) *Eunotia praerupta* present (2.57-2.34 m MTL range)		2.23 ± 0.06	0.00 ± 0.08	
A4-7 (4-5 cm)	2.18	*Eunotia praerupta* falling (2.57-2.34 m MTL range) *Pinnularia intermedia* rising (2.61-2.06 m MTL range) *Nitzschia palea* present (2.41-1.84 m MTL range) *Navicula pusilla* present (2.42-1.98 m MTL range)		2.27 ± 0.15	-0.09 ± 0.16	
A4-9 (4-5 cm)	2.08	*Pinnularia microstauron* present (2.29-1.95 m MTL range) *Pinnularia intermedia* falling (2.61-2.06 m MTL range) *Eunotia praerupta* present (2.57-2.34 m MTL range) *Navicula pusilla* present (2.42-1.98 m MTL range)		2.17 ± 0.12	-0.09 ± 0.13	
A4-10 (3-4 cm)	2.03	*Navicula pusilla* rising (2.42-1.98 m MTL range) *Caloneis borealis* rising (2.19-1.44 m MTL range) *Eunotia praerupta* falling (2.57-2.34 m MTL range)		2.09 ± 0.10	-0.06 ± 0.11	

Table 4 Visual Assessment reconstruction criteria for reconstructing palaeomarsh surface elevation and relative sea level from A4-7 and A4-3. The elevation estimates derived from the diatom data are based on data presented in Figure 4. Height errors are as for Table 3.

Marsh A3						
*A3-3 Lower (6-7 cm)	1.87	*Pinnularia intermedia* falling (2.61-2.06 m MTL range) *Pinnularia microstauron* rising (2.29-1.95 m MTL range) *Navicula pusilla* present (2.42-1.98 m MTL range)	2.13 ± 0.16	-0.34 ± 0.16	2.30 ± 0.20	-0.43 ± 0.21
*A3-3 Upper (4-5 cm)	1.89	*Pinnularia microstauron* falling (2.29-1.95 m MTL range) *Pinnularia intermedia* absent (2.61-2.06 m MTL range)	1.99 ± 0.06	-0.18 ± 0.08	1.83 ± 0.20	0.06 ± 0.21
A3-3 (3-4 cm)	1.90	*Pinnularia microstauron* absent (2.29-1.95 m MTL range) *Pinnularia intermedia* absent (2.61-2.06 m MTL range) *Navicula cincta* rising (rises to peak of 55 % TDV at 1.68 m MTL, with first occurrence >5 % TDV at 2.02 m MTL)	1.82 ± 0.14	0.00 ± 0.08	1.60 ± 0.20	0.33 ± 0.21
A3-3 (2-3 cm)	1.91	*Nitzschia palea* present (2.41-1.84 m MTL range) *Pinnularia microstauron* absent (2.29-1.95 m MTL range)	1.90 ± 0.06	-0.07 ± 0.08	1.74 ± 0.19	0.20 ± 0.20
A3-3 (1-2 cm)	1.92	*Nitzschia palea* present (2.41-1.84 m MTL range) *Pinnularia microstauron* absent (2.29-1.95 m MTL range)	1.90 ± 0.06	-0.06 ± 0.08	1.75 ± 0.19	0.20 ± 0.20
A3-3 (0-1 cm)	1.93	*Nitzschia palea* present (2.41-1.84 m MTL range) *Pinnularia microstauron* absent (2.29-1.95 m MTL range)	1.90 ± 0.06	-0.05 ± 0.08	1.69 ± 0.19	0.27 ± 0..20
Marsh A4						
*A4-7 (4-5 cm)	2.08	*Eunotia praerupta* falling (2.57-2.34 m MTL range) *Pinnularia intermedia* rising (2.61-2.06 m MTL range) *Nitzschia palea* present (2.41-1.84 m MTL range) *Navicula pusilla* present (2.42-1.98 m MTL range)	2.27 ± 0.15	-0.19 ± 0.16	2.26 ± 0.20	-0.08 ± 0.21
A4-7 (3-4 cm)	2.09	*Eunotia praerupta* falling (2.57-2.34 m MTL range) *Pinnularia intermedia* rising (2.61-2.06 m MTL range) *Nitzschia palea* present (2.41-1.84 m MTL range) *Navicula pusilla* present (2.42-1.98 m MTL range)	2.27 ± 0.15	-0.18 ± 0.16	2.25 ± 0.20	-0.13 ± 0.21
A4-7 (2-3 cm)	2.10	*Eunotia praerupta* falling (2.57-2.34 m MTL range) *Pinnularia intermedia* rising (2.61-2.06 m MTL range) *Nitzschia palea* present (2.41-1.84 m MTL range) *Navicula pusilla* present (2.42-1.98 m MTL range)	2.27 ± 0.15	-0.17 ± 0.16	2.17 ± 0.20	-0.04 ± 0.21
A4-7 (1-2 cm)	2.11	*Eunotia praerupta* falling (2.57-2.34 m MTL range) *Pinnularia intermedia* rising (2.61-2.06 m MTL range) *Nitzschia palea* present (2.41-1.84 m MTL range) *Navicula pusilla* present (2.42-1.98 m MTL range)	2.27 ± 0.15	-0.16 ± 0.16	2.22 ± 0.20	-0.08 ± 0.20
A4-7 (0-1 cm)	2.12	*Eunotia praerupta* falling (2.57-2.34 m MTL range) *Pinnularia intermedia* rising (2.61-2.06 m MTL range)	2.27 ± 0.15	-0.16 ± 0.16	2.13 ± 0.20	0.02 ± 0.21

		Nitzschia palea present (2.41-1.84 m MTL range) *Navicula pusilla* present (2.42-1.98 m MTL range)				


a)
Disko Bugt
Jakobshavn Isbrae
b)
Greenland Ice Sheet
Norse West Settlement
Norse East Settlement
Nanortalik
b)
Isunguata Sermia
Sandflugtdalen
Kangerlussuaq
Sisimiut
Søndre Strømfjord
c)
Nagtoralinguaq
820
1030
1230
1100
Sukkertoppen Ice Cap
N
Land over 200 metres
0 km 20
c)
0 km 1
N
d)
d)
A4
A3
A2
A1
NAG-1
N
0 metres 200

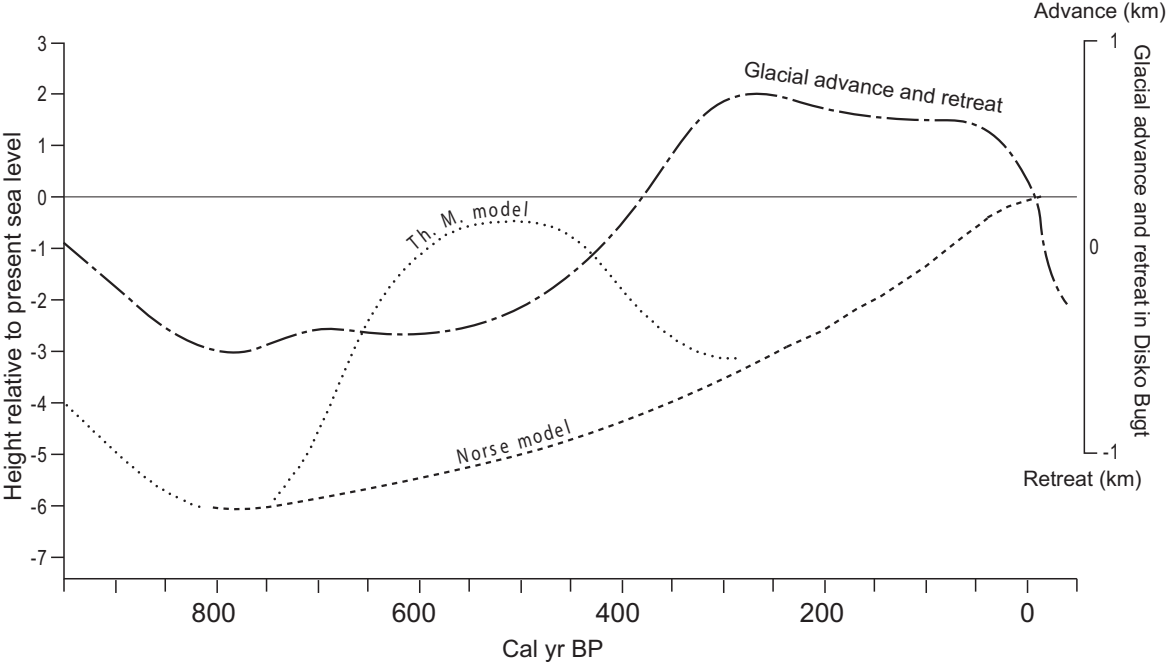
Advance (km)
1
0
-1
Retreat (km)
Glacial advance and retreat in Disko Bugt
Glacial advance and retreat
Th. M. model
Norse model
Height relative to present sea level
3
2
1
0
-1
-2
-3
-4
-5
-6
-7
800
600
400
200
0
Cal yr BP


Marsh A1
Upland
High marsh
High marsh
Exposed bedrock
Low marsh
Tidal flat (submerged)

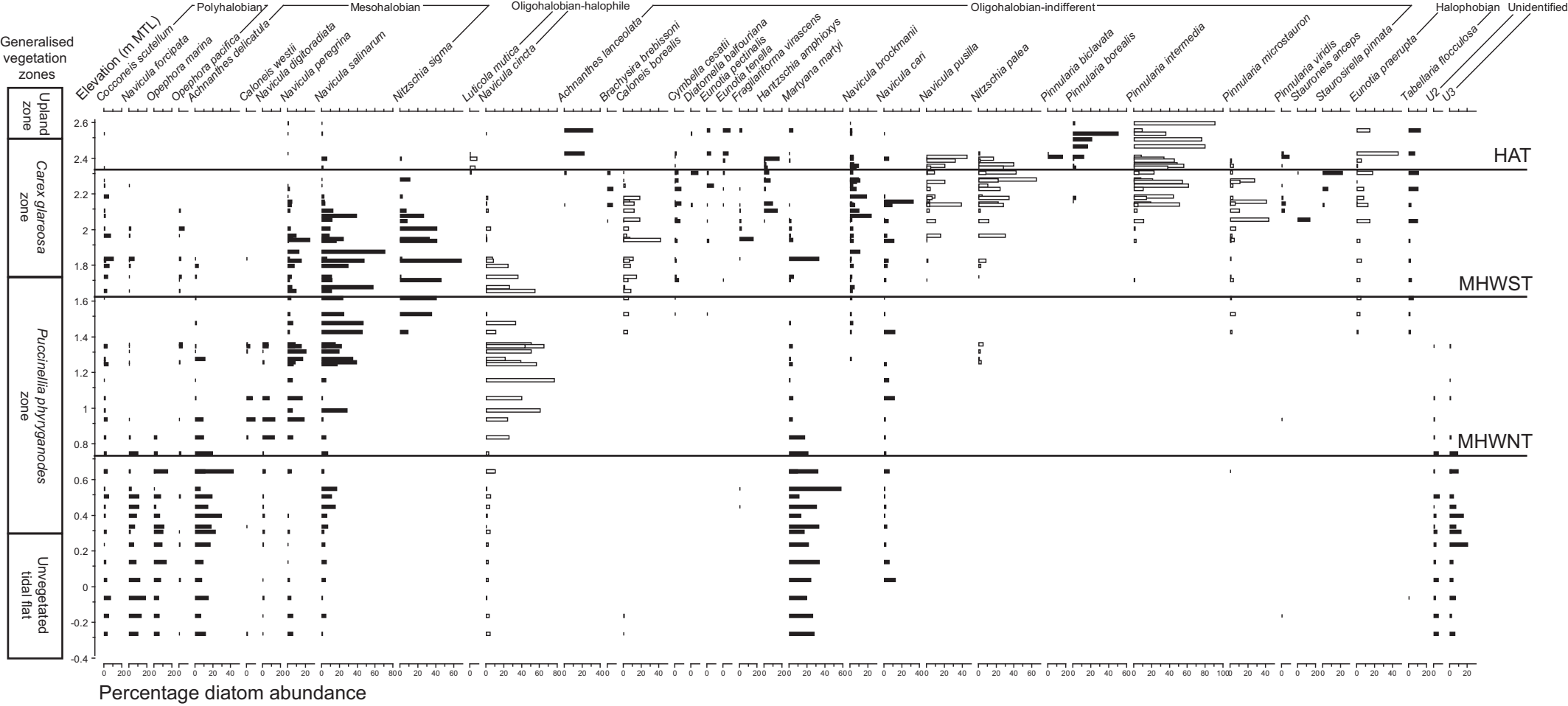
Generalised vegetation zones
Upland zone
Carex glareosa zone
Puccinellia phryganodes zone
Unvegetated tidal flat
Elevation (m MTL)
Polyhalobian
Mesohalobian
Oligohalobian-halophile
Oligohalobian-indifferent
Halophobian
Unidentified
Cocconeis scutellum
Navicula forcipata
Opephora marina
Opephora pacifica
Achnanthes delicatula
Caloneis westii
Navicula digitoradiata
Navicula peregrina
Navicula salinarum
Nitzschia sigma
Luticola mutica
Navicula cincta
Achnanthes lanceolata
Brachysira brebissonii
Caloneis borealis
Cymbella cesatii
Diatomella balfouriana
Eunotia pectinalis
Eunotia tenella
Fragilariforma virescens
Hantzschia amphioxys
Martyana martyi
Navicula brockmanii
Navicula cari
Navicula pusilla
Nitzschia palea
Pinnularia biclavata
Pinnularia borealis
Pinnularia intermedia
Pinnularia microstauron
Pinnularia viridis
Stauroneis anceps
Staurosirella pinnata
Eunotia praerupta
Tabellaria flocculosa
U2
U3
HAT
MHWST
MHWNT
Percentage diatom abundance

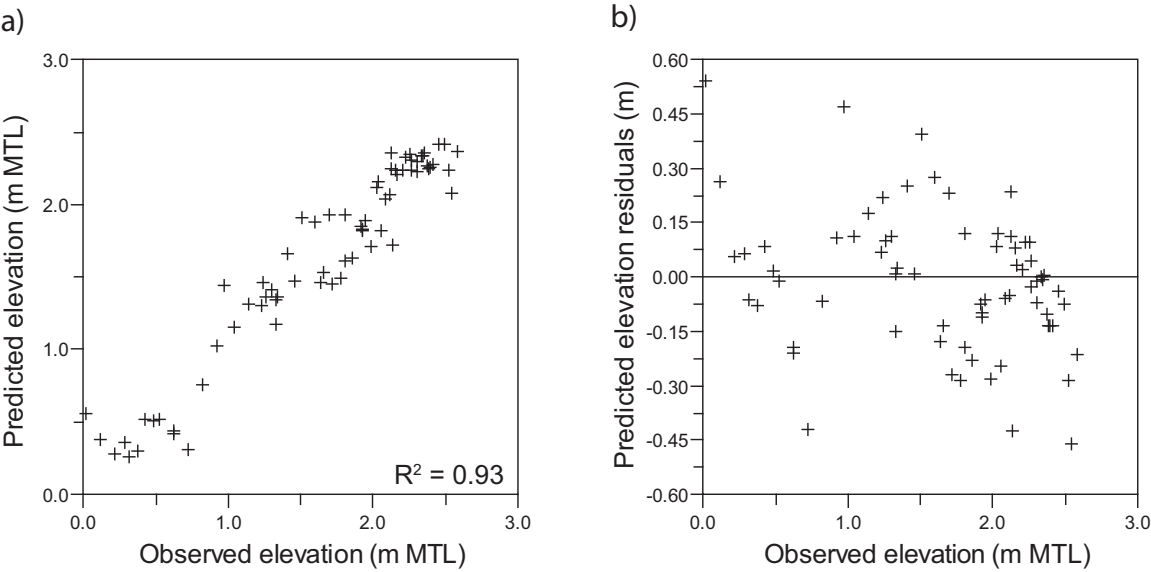
a)
Predicted elevation (m MTL)
Observed elevation (m MTL)
R² = 0.93
0.0
1.0
2.0
3.0
b)
Predicted elevation residuals (m)
Observed elevation (m MTL)
0.60
0.45
0.30
0.15
0.00
-0.15
-0.30
-0.45
-0.60

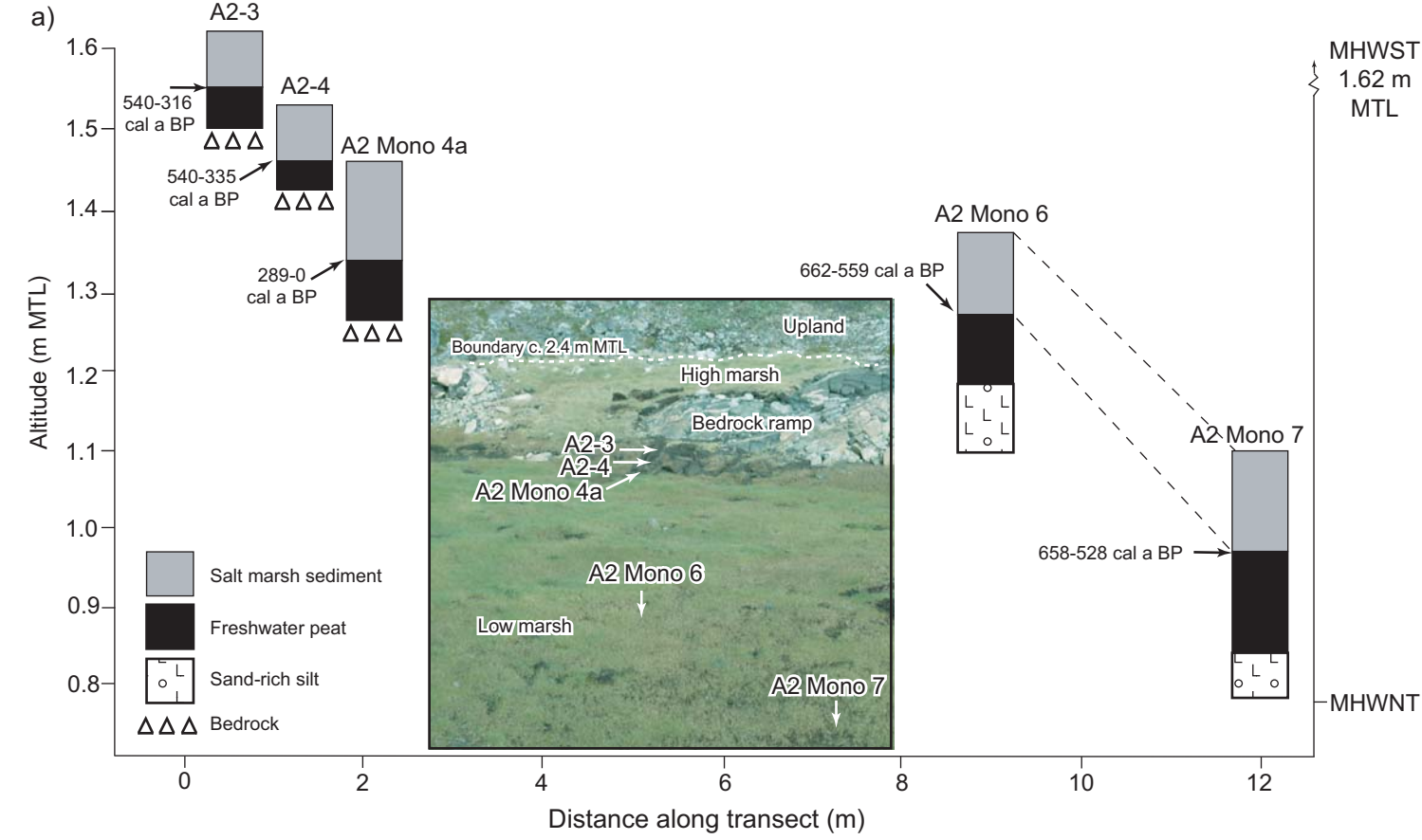
a)
A2-3
A2-4
A2 Mono 4a
A2 Mono 6
A2 Mono 7
540-316 cal a BP
540-335 cal a BP
289-0 cal a BP
662-559 cal a BP
658-528 cal a BP
MHWST 1.62 m MTL
MHWNT
Altitude (m MTL)
Distance along transect (m)
Boundary c. 2.4 m MTL
Upland
High marsh
Bedrock ramp
Low marsh
Salt marsh sediment
Freshwater peat
Sand-rich silt
Bedrock

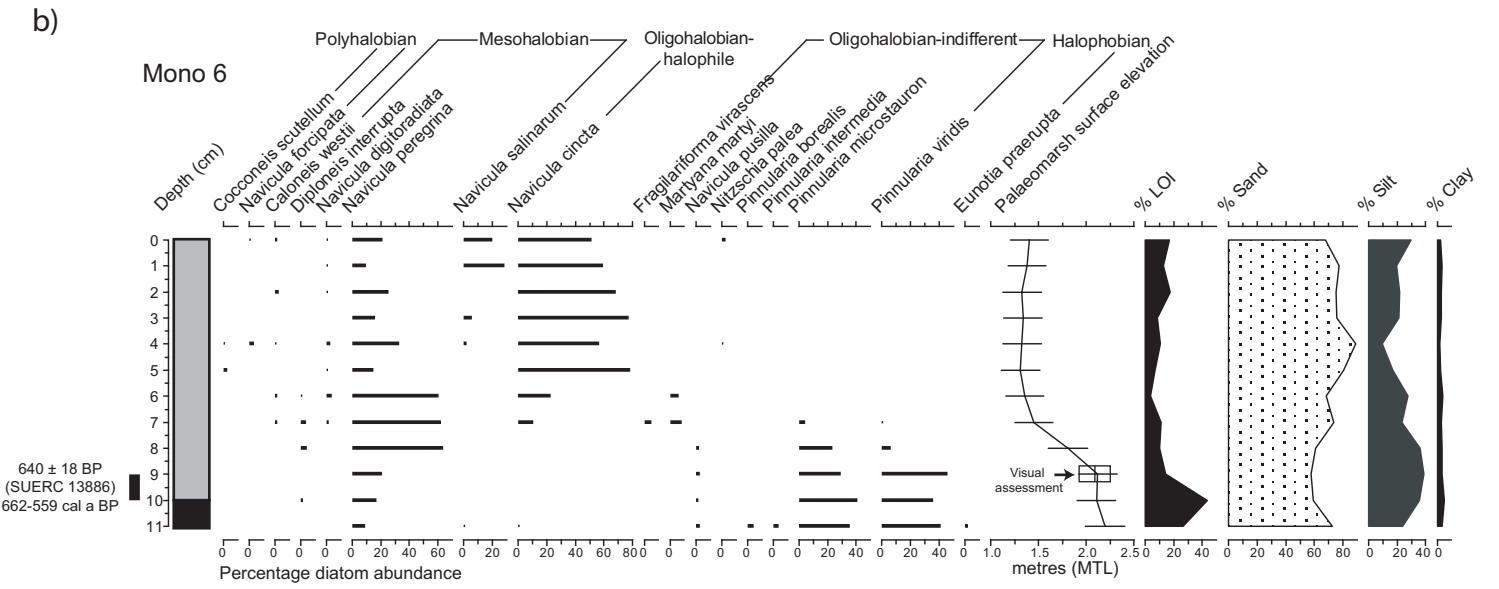
b)
Mono 6
Polyhalobian
Mesohalobian
Oligohalobian-halophile
Oligohalobian-indifferent
Halophobian
Cocconeis scutellum
Navicula forcipata
Caloneis westii
Diploneis interrupta
Navicula digitoradiata
Navicula peregrina
Navicula salinarum
Navicula cincta
Fragilariforma virescens
Martyana martyi
Navicula pusilla
Nitzschia palea
Pinnularia borealis
Pinnularia intermedia
Pinnularia microstauron
Pinnularia viridis
Eunotia praerupta
Palaeomarsh surface elevation
Depth (cm)
% LOI
% Sand
% Silt
% Clay
640 ± 18 BP (SUERC 13886) 662-559 cal a BP
Visual assessment
Percentage diatom abundance
metres (MTL)

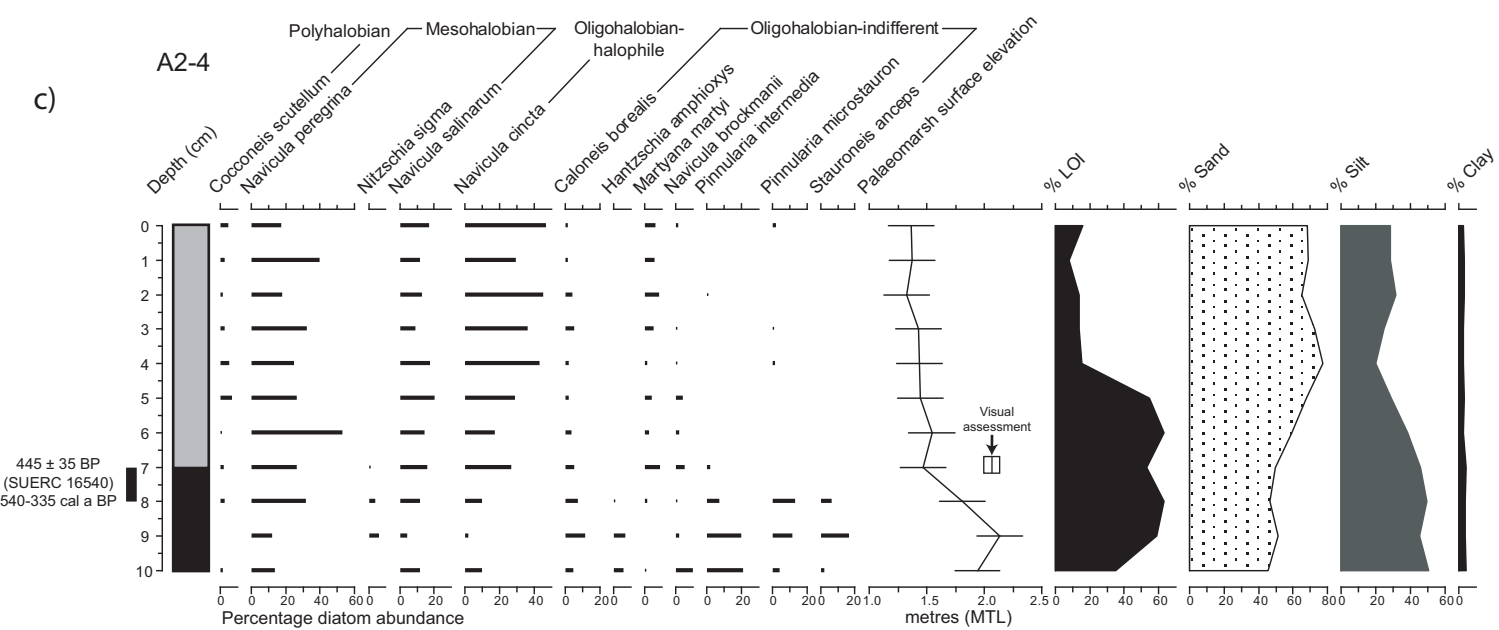
c)
A2-4
Polyhalobian
Mesohalobian
Oligohalobian-halophile
Oligohalobian-indifferent
Cocconeis scutellum
Navicula peregrina
Nitzschia sigma
Navicula salinarum
Navicula cincta
Caloneis borealis
Hantzschia amphioxys
Martyana martyi
Navicula brockmanii
Pinnularia intermedia
Pinnularia microstauron
Stauroneis anceps
Palaeomarsh surface elevation
Depth (cm)
% LOI
% Sand
% Silt
% Clay
445 ± 35 BP (SUERC 16540) 540-335 cal a BP
Visual assessment
Percentage diatom abundance
metres (MTL)

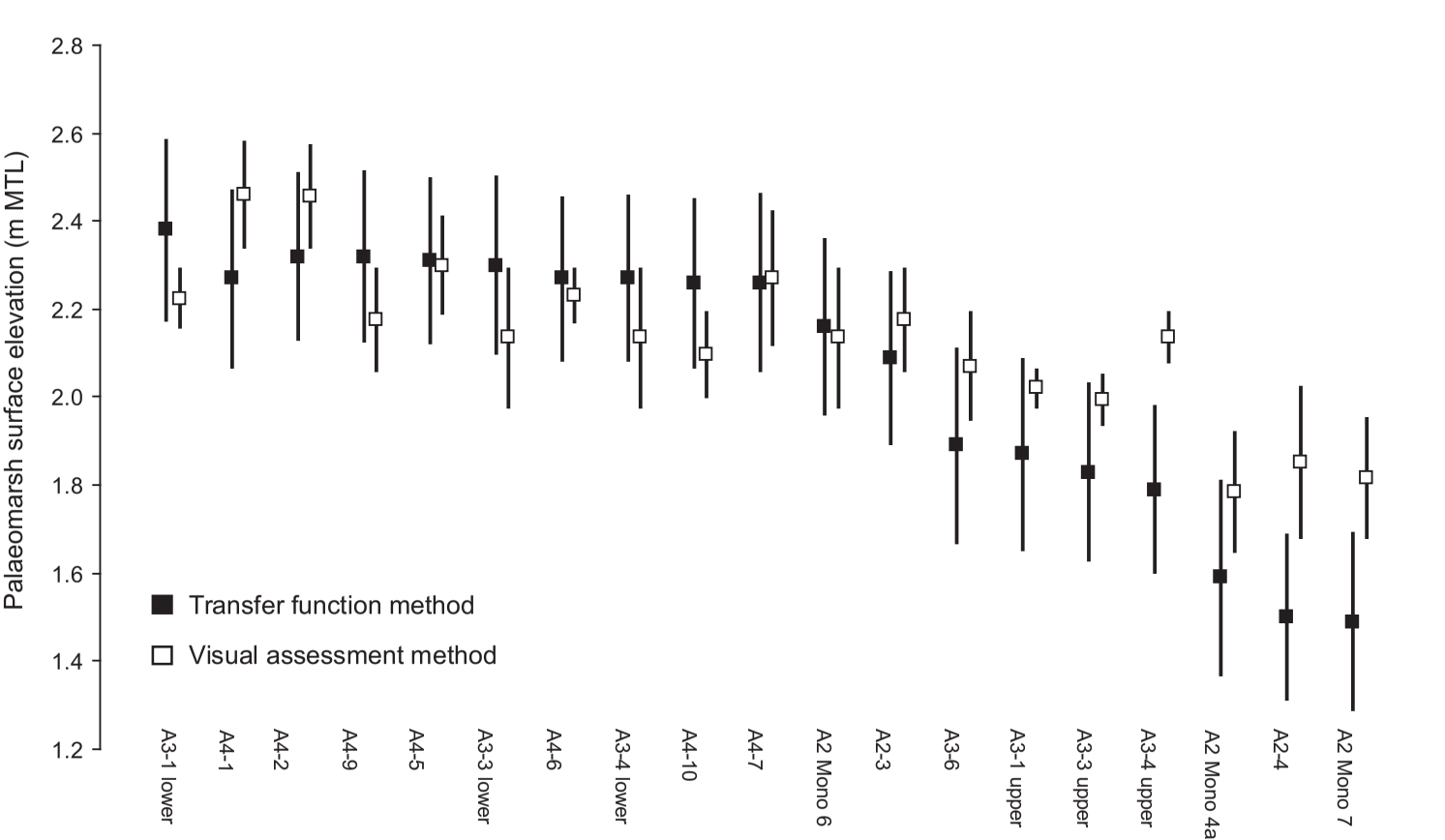
Palaeomarsh surface elevation (m MTL)
2.8
2.6
2.4
2.2
2.0
1.8
1.6
1.4
1.2
Transfer function method
Visual assessment method
A3-1 lower
A4-1
A4-2
A4-9
A4-5
A3-3 lower
A4-6
A3-4 lower
A4-10
A4-7
A2 Mono 6
A2-3
A3-6
A3-1 upper
A3-3 upper
A3-4 upper
A2 Mono 4a
A2-4
A2 Mono 7

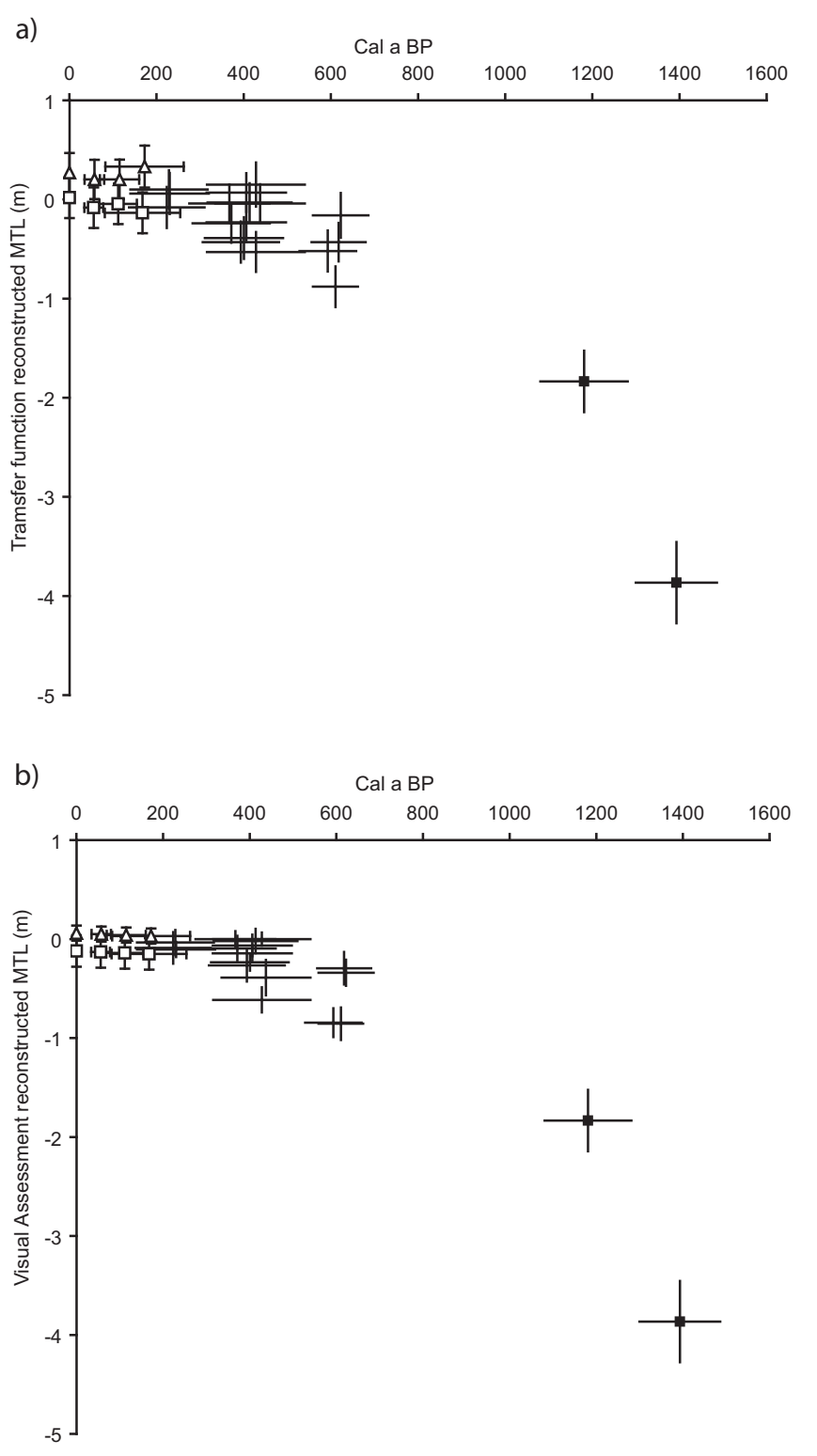
a)
Cal a BP
0
200
400
600
800
1000
1200
1400
1600
1
0
-1
-2
-3
-4
-5
Tramsfer fumction reconstructed MTL (m)
b)
Cal a BP
0
200
400
600
800
1000
1200
1400
1600
1
0
-1
-2
-3
-4
-5
Visual Assessment reconstructed MTL (m)